Global comparison of magnetospheric ion fluxes and auroral precipitation during a substorm

S. B. Mende, H. U. Frey, and T. J. Immel
Space Sciences Laboratory, University of California, Berkeley, CA, USA

D. G. Mitchell and P. C:son-Brandt
The Johns Hopkins University, Laurel, MD, USA

J.-C. Gérard
L'Universitéde Liège, Belgium

Received 20 September 2001; revised 28 February 2002; accepted 12 March 2002; published 29 June 2002.

[1] Integrated fluxes from global images taken by the High Energy Neutral Atom (HENA) and the far ultraviolet (FUV) imagers on the IMAGE spacecraft were compared for a six-hour period, during which a reasonably intense substorm occurred. HENA and the FUV proton auroral imager (SI-12) monitor emissions which are representative of trapped and precipitating magnetospheric proton fluxes, respectively. For several hours prior to substorm onset, measurements of the fluxes of lower energy (10–16 and 16–27 keV) magnetospheric Energetic Neutral Atoms (ENA-s) by HENA and precipitating auroral protons by FUV SI-12 show strong similarities, with the implication that, in general, proton precipitation is controlled by a steady pitch angle diffusion process. Less similarity is seen between ENA-s and the auroral electron precipitation, which is monitored with the FUV Wideband Imaging Camera. Prior to substorm onset, ENA intensity at large radial distance ($L > 8$) is reduced while the overall integrated ENA flux increases signifying earthward motion and accumulation of the plasma. About 20 minutes before onset, the auroral fluxes decrease while the ENA intensity continues to grow. The observations are consistent with a pre-onset increase in plasma pressure in the inner magnetosphere without an increase in precipitation showing more efficient trapping perhaps by the distorted nightside magnetosphere. At substorm onset the increase in precipitation intensity is very sudden while the more gradual intensification of the energetic ENA-s continues. At onset the electron aurora shows an increase in intensity of one order of magnitude, while the increase in precipitating proton flux is only 50%. The intensification of the precipitation is relatively short lived ($\sim$10 minutes) while the ENA substorm enhancements last about an hour. *INDEX TERMS:* 2788 Magnetospheric Physics: Storms and substorms; 2740 Magnetospheric Physics: Magnetospheric configuration and dynamics; 2716 Magnetospheric Physics: Energetic particles, precipitating; 2720 Magnetospheric Physics: Energetic particles, trapped; 2704 Magnetospheric Physics: Auroral phenomena (2407)

1. Introduction

[2] The neutral atom imagers on the IMAGE spacecraft image energetic magnetospheric ions through remote sensing detection of the energetic neutral atoms (ENA-s) produced by charge exchange between the ions and the neutral consituents of the exosphere and upper atmosphere. In principle, ENA measurements allow one to determine the global energetic ion distribution in the magnetosphere [*Roleof*, 1987]. *Henderson et al.* [1997] showed that detectable ENA flux increases occur in response to an individual substorm. *Jorgensen et al.* [2000] were able to systematically associate ENA enhancements with substorms having identified the timing of substorm onsets from satellite based images of the VIS imager on the POLAR satellite and from ground based magnetometer data.

[3] Stably trapped protons on closed field lines are not expected to precipitate because the pitch angle distributions are invariant, and after the initial removal of particles in the loss cone, no more protons reach the atmosphere. It is widely held that magnetospheric trapped protons are a stable population and no precipitation is expected to occur unless there is a mechanism to disturb the particle pitch angle distribution. Significant precipitation can occur when: a) fresh particles of isotropic pitch angle distribution are injected into a region of closed field lines (dayside reconnection or nightside substorm injection process), b) electric fields (dc or wave) interact with stably trapped particles to diffuse them into the loss cone, c) magnetic reconfiguration compresses the volume of the field/flux region (compression) or d) when particles are scattered in stretched field line configurations e.g. during substorm growth phase.

[4] In the analysis of space based auroral images [*Frank and Craven*, 1988; *Murphree et al.*, 1994; *Ephinstone et al.*, 1996; *Germany et al.*, 1997], the auroras produced by precipitating protons were largely ignored. Although low-altitude Earth orbiting satellites have surveyed the average distribution of proton precipitation [e.g. *Hardy et al.*, 1989] the dynamics of global proton precipitation could not be observed prior to the flight of the IMAGE spacecraft. The IMAGE spacecraft carries a set of far ultraviolet (FUV) imagers to monitor the instantaneous auroral distributions consisting of the Wideband Imaging Camera (WIC) and the dual-channel spectrographic imager that images the proton aurora by observing the Doppler shifted Lyman alpha emissions through its SI-12 channel.

0094-8276/02/2001GL014143$05.00

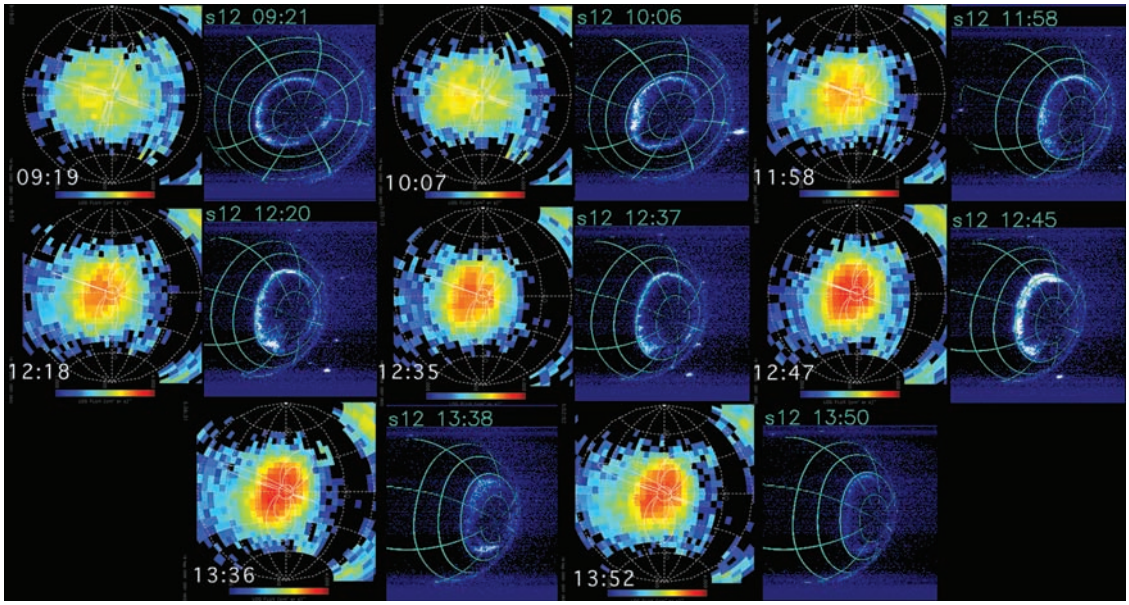

Figure 1. Near simultaneous images taken with the HENA 16–27 keV neutral imaging channel and the IMAGE FUV SI-12.

[5] The high-energy neutral atom imager (HENA) [*Mitchell et al.*, 2000] is able to detect ENA-s in the 10–200 keV range. The magnitude of the observed ENA flux depends on the fluxes of magnetospheric ions, the density of cold neutral gas available for charge exchange, the location of the charge exchange process and the position of the IMAGE spacecraft relative to the direction of the ejected neutrals. This latter factor is important because the distribution of the ejected neutrals is strongly dependent on the pitch angle distribution of the ions. Thus the precise interpretation of the ENA images into magnetospheric ion distributions is a difficult inversion task [*Perez et al.*, 2001].

[6] In spite of these difficulties it is valuable to compare the total flux of ENA-s detected by HENA and the total precipitated auroral fluxes observed by a space based FUV global imager. The ENA images are primarily representative of the ion distribution of the trapped fluxes in the magnetosphere while the proton aurora measured by the SI-12 instrument represents the precipitating component. Since the IMAGE spacecraft carries imagers which can separate electron and proton precipitation, it provides an opportunity to compare the variability of the total trapped flux to the precipitated flux on a global basis.

2. Observations

[7] Between 0830 and 1430 UT on September 19th, 2000 the IMF, (WIND $x_{GSM} = +34R_e$, $-v_{sw} = 650$ km s^{-1}) data showed that B_z was fluctuating between 0 to −5 and B_y was strongly negative until about 1240 when it became positive. The auroral situation can be seen by examining the IMAGE WIC images for day 263, 2000 displayed at http://sprg.ssl.berkeley.edu/image/wic_summary. From the WIC images it can be seen that several substorm-like events occurred. One minor event started around 0950 and lasted until about 1050 UT. A major event occurred around 1240 UT which could have been triggered by the IMF field change mentioned above.

[8] Images taken simultaneously with the HENA 16–27 keV neutral imaging channel and the IMAGE FUV SI-12 channel are illustrated in Figure 1. During these observations the composition resolving capability of the HENA imager was not active. The IMAGE satellite was located approximately above the North Pole. On the ENA images the field lines at L = 4 and L = 8 are illustrated at 00, 06,12 and 18 hours magnetic local time. The sunward direction (12 MLT) in all SI-12 and HENA images is towards the right and slightly down. The SI-12 images are marked with contours of 30°, 45°, 60° and 75° magnetic latitude and local times of 00, 03, 06, 09, 12, 15, 18, 21 hours. To mark the midday 12 MLT meridian the 45° magnetic latitude contour was thickened at the intersection with the 12 MLT meridian (right on the 09:21 image slightly below horizontal). Since the IMAGE spacecraft is in a true polar orbit with its spin axis normal to the orbit plane, the azimuthal position of the MLT contours do not change significantly from the beginning to the end of this observation period. The reader should note that the ENA images have not been inverted and the intensity seen at a pixel located at geocentric radius R on the picture has contributions along the line of sight from regions in space whose geocentric radius is R or greater. Furthermore, and more importantly, the representation of the magnetospheric ion distribution by ENA images is greatly distorted by the large radial variations in the exospheric neutral densities available for charge exchange. So ENA-s tend to originate from a volume of space very near the earth (∼2–3 Re), even while they represent trapped ion fluxes that uniformly populate field lines of L values >4.

[9] In Figure 2 we have illustrated the integrated ENA flux data as a function of time including the FUV SI-12 and WIC data. The ENA flux has been summed over the field of view, which is ±30 degrees latitude and the 0 and 30

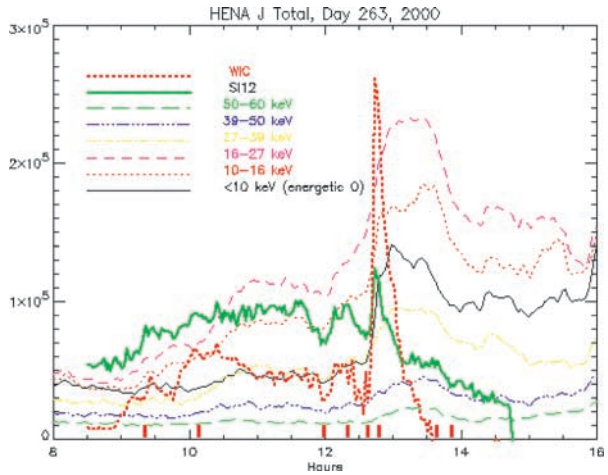

Figure 2. Intensity versus time plots for all HENA channels and the integrated image FUV SI-12 and WIC. Short vertical bars show time of images in Figure 1.

degrees of longitude in HENA instrument centered look angle coordinates. Six curves represent the sum of the instrument counts at different energy ranges from the HENA time of flight energy channels 50–60, 39–50, 27–39, 16–27, 10–16 and 0–10 keV. The thick solid green line is the integrated proton aurora over the entire northern auroral region. This was obtained by integrating the SI-12 photo-electron counts between magnetic latitude of 55 and 80 degrees. A background subtraction was performed by integrating the counts in the region of magnetic latitude greater than 80 and normalizing the result for the size of the area of the region between 55 and 80 degrees. The red dotted line is the IMAGE WIC AD (analog-to digital converted CCD signal) units which were also integrated in the 55–80° magnetic latitude region but only on the night side (MLT > 1800 and MLT < 0600) to avoid the complexities of dayglow corrections. In prior work comparing ENA with ultraviolet auroral imaging (e.g. *Henderson et al.* [2000]) the aurora was observed with instruments whose responsivity was dominated by emission caused by electron precipitation, which is the case with the WIC images.

3. Discussion

[10] At 0920 the lower energy channels of HENA (< 27 keV) show a significant increase, which is matched by a 50% increase in SI-12 response (green solid line). From this time to 0950 UT, the proton flux is relatively steady. A gradual increase is observed in the WIC channel at 0950 (red dotted line) presumably due to the spatial expansion of the surge like feature seen in the WIC images (not shown). Unlike the earlier increase in proton emissions, there is no observable change in ENA production associated with this.

[11] After 0950 UT, the proton flux climbs again together with the ENA fluxes in all channels until 1140 UT. The integrated counting rates from WIC drop steadily throughout the 1000–1200 UT period. Precipitating fluxes and low energy ENA-s reach a minimum at 1200 UT. In Figure 1 the ENA images labeled 11:58 and 12:18 show increased intensity on the night side at L = 8 and larger. In the later images (12:35 and 12:47) this region is depleted while the integrated 16–27 keV ENA fluxes are actually increasing (dashed line Figure 2). This can be interpreted as an inward motion of the nightside plasma occurring prior to the onset of the substorm at 1240. Between 1200 and 1240 UT, the precipitating proton and electron fluxes undergo a dramatic variation, first dropping rapidly, then rising again to peak around 1220 thereafter dropping again until the onset at 1240. The ENA fluxes do not vary as rapidly, but the low energy channels also have a minimum at 1200 in correspondence with the SI-12. After 1200 the ENA fluxes start climbing through the period when the precipitating fluxes decrease. The increase continues through the main expansion which is observed in the FUV channels at 1240.

[12] At 1240, the main expansion of the aurora occurs, where the proton fluxes nearly double, the electron fluxes increase by a decade, and the ENA fluxes all continue to rise. Compared to the auroral precipitation, the ENA-s are slow to rise and the precipitating fluxes have dropped below all pre-onset values by the time the ENA fluxes finally peak. During the onset the lowest energy ENA < 10 keV channel (black solid line) shows the greatest similarity to the precipitating flux. It is likely that the lowest energy ENA-s were actually oxygen atoms in the 80 to 150 keV energy range [*Mitchell et al.*, 2001]. If they are oxygen, then the similarity of the plot to that of the precipitating particles suggests that these particles, which originate from the ionosphere, have undergone acceleration and/or pitch-angle scattering immediately at substorm onset.

[13] In the following period (UT > 1250) the time history of the SI-12 and WIC fluxes differs from that of the ENA showing that the precipitating proton or electron fluxes differ from the trapped ion fluxes at all energies. In Figure 1 the image pairs were selected to illustrate the most important features of the intensity plots of Figure 2. The increase in the integrated ENA counts in the lower energy channels at 0920 and the accompanied increase in the global proton SI-12 auroral intensity is shown in the image pair (ENA at 09:19 and SI-12 at 09:21 on Figure 1). This shows weak proton auroras and ENA-s in the green-yellow intensity range. The gradual increase in the ENA-s culminates around 1100, proceeding then to a minimum at 1200. This drop is considerably more explicit in the precipitating particles showing that the proton aurora is very narrow in the dusk region (Figure 1 at 11:58). At this time a small region of ENA enhancement seems to create a slight color change in the center of the ENA image. After 1200 there is a flux increase in both the lowest energy ENA-s and the precipitating fluxes which reach a maximum at about 1220. The ENA image shows a much larger orange-yellow area at 12:18 and the proton auroral activity is much more extensive in local time. The ENA fluxes keep increasing through the substorm onset at 1240. The precipitating fluxes measured by both SI-12 and WIC show a substantial drop prior to onset (See image pair at 12:35 and 12:37). At the onset when the integrated WIC signal increases by an order of magnitude, the HENA-SI-12 image pair at 12:47 and 12:45 shows that the ENA image turned red and the entire night side oval "lit up" with proton aurora. According to Figure 2 the ENA fluxes increase much more slowly than the protons and by 13:38 the precipitating proton fluxes weaken while enhanced ENA fluxes on the night side of the ENA image (at 13:36) remain. The image pair at 13:50 and 13:52 denotes the end of

the intense proton auroras and shows a slight decrease in the ENA-s.

4. Summary

[14] Both measurements, ENA and FUV, are imperfect indicators of magnetospheric particle fluxes for reasons discussed in the introduction. However the following observations were made: In the period preceding the substorm for several hours the gross features of the ENA flux and SI-12 proton integrated curves are quite similar. This shows that in general magnetospheric proton precipitation is controlled by steady pitch angle diffusion processes. The similarity with the lower energy (10–16 and 16–27 keV) ENA channels is particularly striking as there is less similarity between ENA-s and WIC measurements which represent mainly electron produced auroras.

[15] The auroral onset in both WIC and SI-12 data is preceded by the decrease of the $L > 8$ fluxes on the nightside between 12:20 and 12:45 UT. These ions produce relatively few ENA-s because of the lack of exospheric neutrals at large geocentric radial distances but as the ions are driven towards the earth into regions of high neutral density more intense ENA fluxes are produced. Thus, the data shows evidence for the plasma being driven earthward prior to substorm onset.

[16] Just prior to the substorm expansive phase (in the growth phase) the precipitated fluxes reach a minimum while the ENA-s show a slight growth. The sudden drop in total auroral luminosity prior to substorm onset has been documented by prior studies, however our observation of the global proton auroral behavior is new. It is also very interesting that prior to substorm onset the precipitation of both protons and electrons decreased, while the trapped particle fluxes were increasing.

[17] Thus, during the pre-substorm growth phase the total ENA-s signify a plasma pressure increase in the inner magnetosphere which is not accompanied by an increase in precipitation. The decrease of precipitation with the apparent increase in trapped particles can be explained by the large B_i / B_e (ionospheric/equatorial) ratios of the extended field lines in the near tail region. An alternate explanation to a plasma density increase could be that the magnetic field configuration change enhanced the receptions of ENA-s at IMAGE giving a false interpretation of flux increase.

[18] At substorm onset the change in intensity of the auroral protons and electrons is very sudden while the intensification of the near earth ENA-s is much more gradual. (Note that the rapidly responding lowest energy ENA channel is known to have significant high energy O contribution.) The sudden increase in the precipitating flux shows that the initially injected particles tend to have more particles in the loss cone than those which are injected later.

[19] The rapid intensification of precipitating electrons and protons with substorm onset is short lived ($\sim$10 minutes) while the ENA enhancements are long lived (lasting almost a whole hour). This can be explained on the basis of the protons being very stably trapped after the substorm initial expansive phase is finished. In the stable configuration the pitch angle diffusion is slow yielding only a few particles in the loss cone.

[20] Independent of the ENA measurements, IMAGE FUV data present a good example of a typical substorm expansive phase showing that while the intensity of the electrons suddenly increases one whole order of magnitude the protons increase modestly, only about 50%. It will be important in the future to conduct several such case studies to show that these conclusions represent typical substorm behavior.

[21] **Acknowledgments.** The WIND IMF data was provided by Dr. R. Lepping of NASA/GSFC and was obtained through CDAWEB. This work was supported through SWRI subcontract number 83820 at the University of California, Berkeley, and by NASA under contract number NAS5-96020 and J.-C. Gérard is supported by the Belgian FNRS and funded for this research by the PRODEX program of ESA.

References

Ephinstone, R. D., J. S. Murphree, and L. L. Cogger, What is a global substorm?, *Rev. Geophys.*, *34*, 169, 1996.

Frank, L. A., and J. D. Craven, Imaging results from Dynamics Explorer 1, *Rev. Geophys.*, *2*, 249, 1988.

Germany, G. A., G. K. Parks, M. Brittnacher, J. Cumnock, D. Lummerzheim, J. F. Spann, L. Chen, P. G. Richards, and F. J. Rich, Remote determination of auroral energy characteristics during substorm activity, *Geophys. Res. Lett.*, *8*, 995, 1997.

Hardy, D. A., M. S. Gussenhoven, and D. Brautigam, A statistical model of auroral ion precipitation, *J. Geophys. Res.*, *94*, 370, 1989.

Henderson, M. G., G. D. Reeves, H. E. Spence, R. B. Sheldon, A. M. Jorgensen, J. B. Blake, and J. F. Fennell, First energetic neutral atom images from Polar, *Geophys. Res. Lett.*, *10*, 1167, 1997.

Henderson, M. G., et al., Polar CEPPAD/IPS energetic neutral atom (ENA) images of a substorm injection, *Adv. Space Res.*, *25*, 2407, 2000.

Jorgensen, A. M., L. Kepko, M. G. Henderson, H. E. Spence, G. D. Reeves, J. B. Sigwarth, and L. A. Frank, Association of energetic neutral atom bursts and magnetospheric substorms, *J. Geophys. Res.*, *105*, 18,753, 2000.

Mitchell, D. G., et al., High energy neutral atom (HENA) imager for the IMAGE mission, *Space Sci. Rev.*, *91*, 67, 2000.

Mitchell, D. G., P. C. Brandt, and D. C. Hamilton, Composition measurements of energetic neutral atoms using the IMAGE/HENA sensor (Abstract), *Eos Trans. AGU*, *82*(47), Suppl., 2001.

Murphree, J. S., M. L. Johnson, L. L. Cogger, and D. J. Hearn, Freja UV imager observations of spatially periodic auroral distortions, *Geophys. Res. Lett.*, *21*, 1887, 1994.

Perez, J. D., et al., Initial ion equatorial pitch angle distributions from medium and high energy neutral atom images obtained by IMAGE, *Geophys. Res. Lett.*, *28*, 1155, 2001.

Roleof, E. C., Energetic neutral atom image of a storm time ring current, *Geophys. Res. Lett.*, *14*, 652, 1987.

S. B. Mende, H. U. Frey, and T. J. Immel, Space Sciences Laboratory, University of California, Berkeley, CA 94720, USA. (mende@ssl.berkeley.edu)

D. G. Mitchell and P. C:son-Brandt, The Johns Hopkins University, Laurel, MD 20723, USA.

J.-C. Gérard, L'Université de Liège, Belgium.